

1
2
3
4
5
6
7
8
9
10
11
12
13
14
15
16
17
18
19
20
21
22

A high pressure oxidation study of di-n-propyl ether

Zeynep Serinyel*^{1,2}, Maxence Lailliau^{1,2}, Guillaume Dayma^{1,2}, and Philippe Dagaut²

¹ Collegium Sciences et Techniques, Université d'Orléans, rue de Chartres, 45100 Orléans

² CNRS-ICARE, 1C avenue de la Recherche Scientifique, 45071 Orléans cedex 2

*Corresponding author:

Zeynep Serinyel, PhD

CNRS-ICARE, Institut de Combustion, Aérodynamique, Réactivité et Environnement

1C Avenue de la Recherche Scientifique

45071 Orléans Cedex 2, France

Tel : +33 (0)2 38 25 77 77

zeynep.serinyel@cnrs-orleans.fr

23 **Abstract**

24 The oxidation of di-n-propyl-ether (DPE), was studied in a jet-stirred reactor. Fuel-lean,
25 stoichiometric and fuel-rich mixtures ($\phi = 0.5-4$) were oxidized at a constant fuel mole
26 fraction of 1000 ppm, at temperatures ranging from 470 to 1160 K, at 10 atm, and constant
27 residence time of 700 ms. The mole fraction profiles were obtained through sonic probe
28 sampling and gas chromatography and Fourier transform infrared spectrometry analyses. As
29 was the case in our previous studies on ethers (diethyl ether and di-n-butyl ether), the carbon
30 neighboring the ether group was found to be the most favorable site for H-abstraction
31 reactions and the chemistry of the corresponding fuel radical drives the overall reactivity. The
32 fuel concentration profiles indicated strong low-temperature chemistry. A kinetic sub-
33 mechanism is developed based on rules similar to those for the two symmetric ethers
34 previously investigated (DEE and DBE). The proposed mechanism shows good performances
35 in representing the present experimental data, nevertheless, more data such as atmospheric
36 pressure speciation will be needed in order to better interpret the kinetic behavior of DPE.

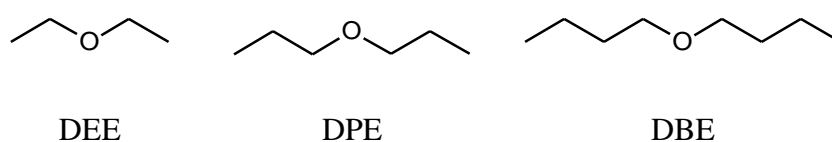
37

38 **Introduction**

39 Given the strict emission regulations for automotive sector and environmental concerns, there
40 has recently been a growing need to find alternative feedstocks for the next generation
41 biofuels. These include di-n-butyl ether (DBE, $C_4H_9-O-C_4H_9$), diethyl ether (DEE, C_2H_5-O-
42 C_2H_5), and dimethyl ether (DME, CH_3-O-CH_3) among many other families of oxygenated
43 molecules. DBE can be produced from lignocellulosic source, while DEE can be produced
44 from bioethanol by dehydration. Very recently, DBE and DEE received a lot of interest. They
45 were studied in different laboratory set-ups, in terms of oxidation, pyrolysis, ignition delays,
46 laminar flame speeds, and laminar flame structure [1-8].

47 Our team has recently studied the oxidation of DBE and DEE in jet-stirred reactor [6,
48 9]. An unusual oxidation behavior showing double-NTC region was observed with DBE,
49 which was not the case with DEE under the same conditions, the latter having shown
50 conventional low-temperature reactivity. Di-n-propyl ether (DPE, $C_3H_7-O-C_3H_7$), on the
51 other hand, is not considered a potential biofuel and has not been studied in combustion.
52 However, in terms of carbon number, this symmetric ether is between DEE and DBE. It is
53 therefore of fundamental interest to study its oxidation behavior. The structures of these ethers
54 are shown in figure 1.

55



56

Figure 1. Structures of diethyl, di-n-propyl and di-n-butyl ethers

57

58 Oxidation of DPE, is therefore studied in the same experimental conditions as DEE and DBE,
59 10 atm, between 470 to 1160 K. A kinetic sub-model is developed for this fuel and compared
60 to the present data only, given that this study is the first investigating di-n-propyl ether
61 oxidation.

62

63 **Experimental approach**

64 Experiments were carried out in a fused silica jet-stirred reactor settled inside a stainless-steel
65 pressure resistant jacket. An electrical oven enabled to perform experiments up to c.a. 1280K.

66 The temperature within the reactor was continuously monitored by a Pt/Pt-Rh thermocouple
67 located inside a thin wall fused silica tube to prevent catalytic reactions on the metallic wires.

68 Initial fuel mole fraction was 1000 ppm for all experiments, pressure and residence time (τ)
69 were held constant 10 atm and 0.7s. The reactive mixtures were highly diluted by nitrogen to

70 avoid high heat release inside the reactor and experiments were performed at temperatures
71 ranging from 450 to 1160 K similar to our previous studies [6, 9]. The liquid fuel was
72 atomized by a nitrogen flow and vaporized through a heated chamber. Reactants were brought
73 separately to the reactor to avoid premature reactions and then injected by 4 injectors
74 providing stirring. Flow rates of the diluent and reactants were controlled by mass
75 flowmeters. A low-pressure sonic probe was used to freeze the reactions and take samples of
76 the reacting mixtures.

77 Online analyses were performed after sending the samples via a heated line to a Fourier
78 transform infrared (FTIR) spectrometer for the quantification of H₂O, CO, CO₂, and CH₂O.
79 Samples were also stored at ca. 40 mbar in Pyrex bulbs for further analyses using gas
80 chromatography (GC). Two gas chromatographs with a flame ionization detector (FID) were
81 used: one equipped with a DB624 column to quantify oxygenated compounds and the other
82 one with a CP-Al₂O₃/KCl column to quantify hydrocarbons. Identification of the products
83 was done by GC/MS on a Shimadzu GC2010 Plus, with electron impact (70 eV) as the
84 ionization mode. Hydrogen profiles were measured using a GC-TCD (thermal conductivity
85 detector) equipped with a CP-CarboPLOT P7 column. The species quantified in this study
86 include di-n-propyl-ether (DPE), H₂, H₂O, CO, CO₂, C₂H₄, CH₄, C₂H₆, C₃H₆, formaldehyde,
87 propanal, acetaldehyde, and propanoic acid. Some other minor oxygenated species were also
88 identified, such as 2-ethyl-4-methyl-1,3-dioxolane, 2-(propoxymethyl)oxirane, and traces of
89 propyl formate and ethyl formate. The cyclic ethers cited are proper to DPE low-temperature
90 chemistry, and they are formed in trace amounts. A quantification is therefore not done, also
91 including the fact that these species were not directly calibrated and that we did not prefer to
92 use an effective carbon method for molar fractions of few ppm. The carbon balance was
93 checked for each sample and was found to be typically within ±10–15%.

94

95 **Kinetic modeling**

96 As the study of DPE is in line with our previous studies on diethyl ether (DEE) and di-n-butyl
97 ether (DBE), a sub-mechanism was developed in a similar way to those of DEE and DBE and
98 integrated into the mechanism as provided in [6]. In the present DPE sub-mechanism, rate
99 constants of the main reactions were adopted from the literature, as follows:

100 - Reactions of hydrogen abstraction from fuel by OH radicals are taken from Zhou et al. [10]
101 for the alpha C–H site. For the beta C–H site, the rate constant is evaluated by fitting to the
102 theoretical calculations performed by [11-13] for the beta C–H in n-butanol. For the gamma
103 C–H site, the rate constant is also assigned by fitting to the calculations of [11-13] and the
104 measurements of Droege and Tully [14] for the delta C–H bond in n-butanol, as this one is the
105 further away from the alcoholic carbon.

106 - Reactions of hydrogen abstraction from fuel by H atoms are taken from the theoretical study
107 of Ogura et al. [15] for the alpha site. For the beta and gamma C–H bonds, rate constants are
108 adopted from Tsang [16].

109 - H-abstraction rate constants by HO₂ and CH₃ radicals are adopted from the theoretical
110 studies of Mendes et al. [17] and Xu et al. [18], respectively.

111 - Rate constants for R+O₂ ⇌ RO₂ reactions are adopted from Goldsmith et al. [19], both for
112 1st and 2nd addition.

113 - Rate constants for RO₂ ⇌ QOOH, QOOH ⇌ cyclic ether + OH are adopted from Villano et
114 al. [20, 21].

115 - Beta-scission reactions of fuel radicals and those of QOOH radicals are adopted from the
116 theoretical calculations of Villano et al. [21], Sakai et al. [22], and from our previous
117 calculations on DBE [9].

118 - Other reactions related to low-temperature chemistry are taken analogous to our previous
119 DBE model [9].

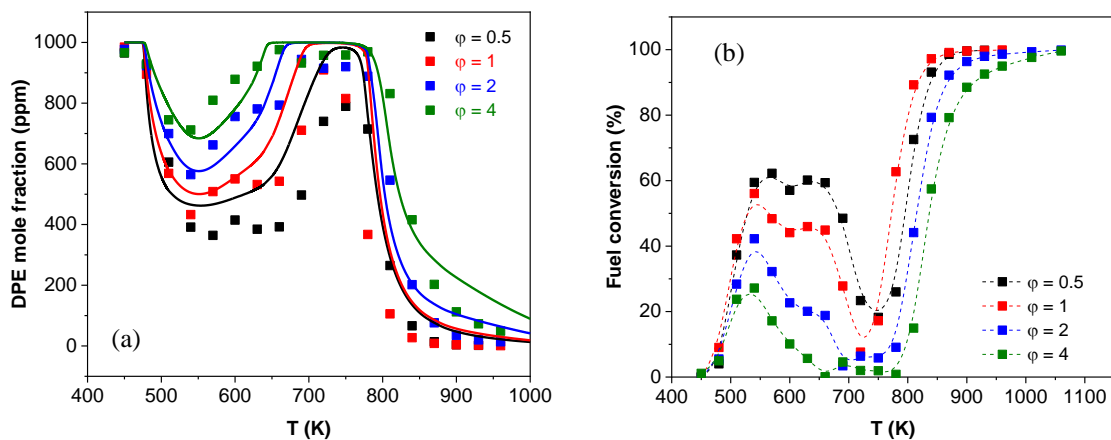
120 - Unimolecular decomposition reactions of DPE were taken from the study of Yasunaga et al.
121 [1] in analogy with DEE. These reactions have no importance under present experimental
122 conditions.

123 Thermochemistry of the fuel, fuel radical as well as all related low-temperature species
124 were calculated using Thergas [23] which uses group additivity methods as proposed by
125 Benson [24]. The JSR simulations were carried out with the Perfectly Stirred Reactor (PSR)
126 code of Chemkin II package [25]. Results are shown in the following figures.

127

128 Results and discussion

129 Fuel conversion and fuel mole fractions for all experiments are presented in Figure 1.



130

131 **Figure 1.** DPE mole fraction profiles (a) and conversion (b) for all mixtures

132

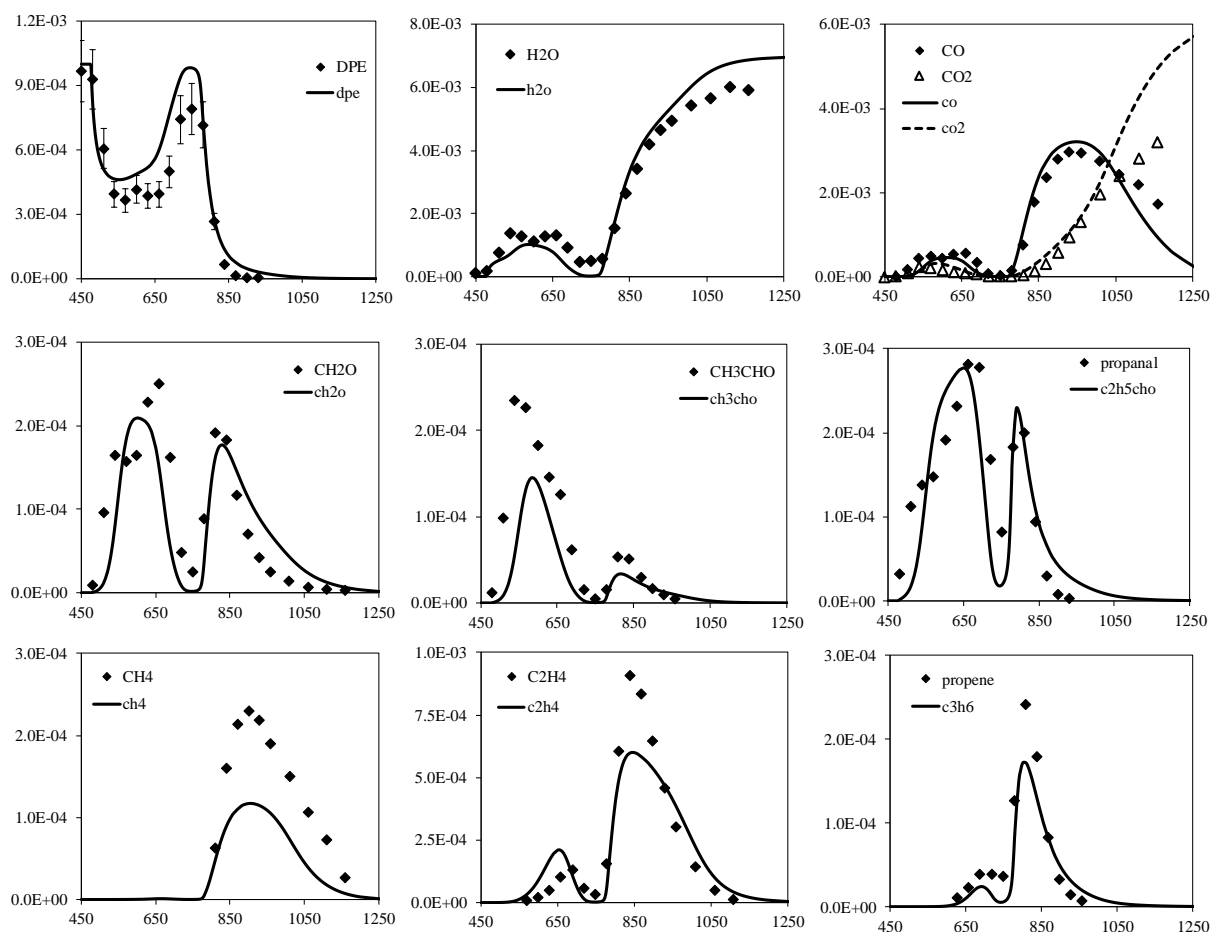
133 DPE shows a strongly pronounced low-temperature reactivity, followed by an NTC region
134 (Figure 1a). For example, the NTC region for the $\phi = 1$ and 2 mixtures, begin around 530 K
135 and arrive to a plateau around 600 K. Then within a temperature window of ~ 60 K, no further
136 fuel conversion is observed, and past 660 K reactivity decreases again. This behavior

137 resembles what was previously observed in DBE oxidation as double-NTC [9], better
138 demonstrated in Figure 1b. For the $\phi = 0.5$ mixture, it would not be adequate to reach this
139 conclusion as the single experimental point (600 K) that could prove this behavior is within
140 experimental uncertainty. On the other hand, the $\phi = 4$ mixture does not show this behavior,
141 also the temperature zone between the end of NTC and start of high-temperature reactivity is
142 wider for this mixture, and approaches zero between 660–780 K.

143 The kinetic model can predict the NTC behavior except for the “2nd NTC” region,
144 although a small difference in the slope can be observed for the lean mixture. These kinetic
145 uncertainties are due to the rate constants adopted in the low-temperature oxidation
146 mechanism. Often, these rate constants are more adequate for alkane oxidation and analogies
147 have to be made in developing mechanisms for oxygenated compounds. The effect of some of
148 these rate constants will be illustrated in the coming sections.

149 In the following figures (2–5), experimental results are presented along with
150 simulations, a representative 15% uncertainty bar is added to the fuel profile. General
151 tendency is well predicted by the model, some discrepancies exist due to the chosen rate
152 constants in low-temperature oxidation sub-mechanism. From Figure 1, one can speculate that
153 the model slightly under-predicts the experimental reactivity of the $\phi = 0.5$ and 1 mixtures in
154 the NTC region.

155



156

157 **Figure 2.** Mole fraction profiles as a function of reactor temperature ($\phi = 0.5$)

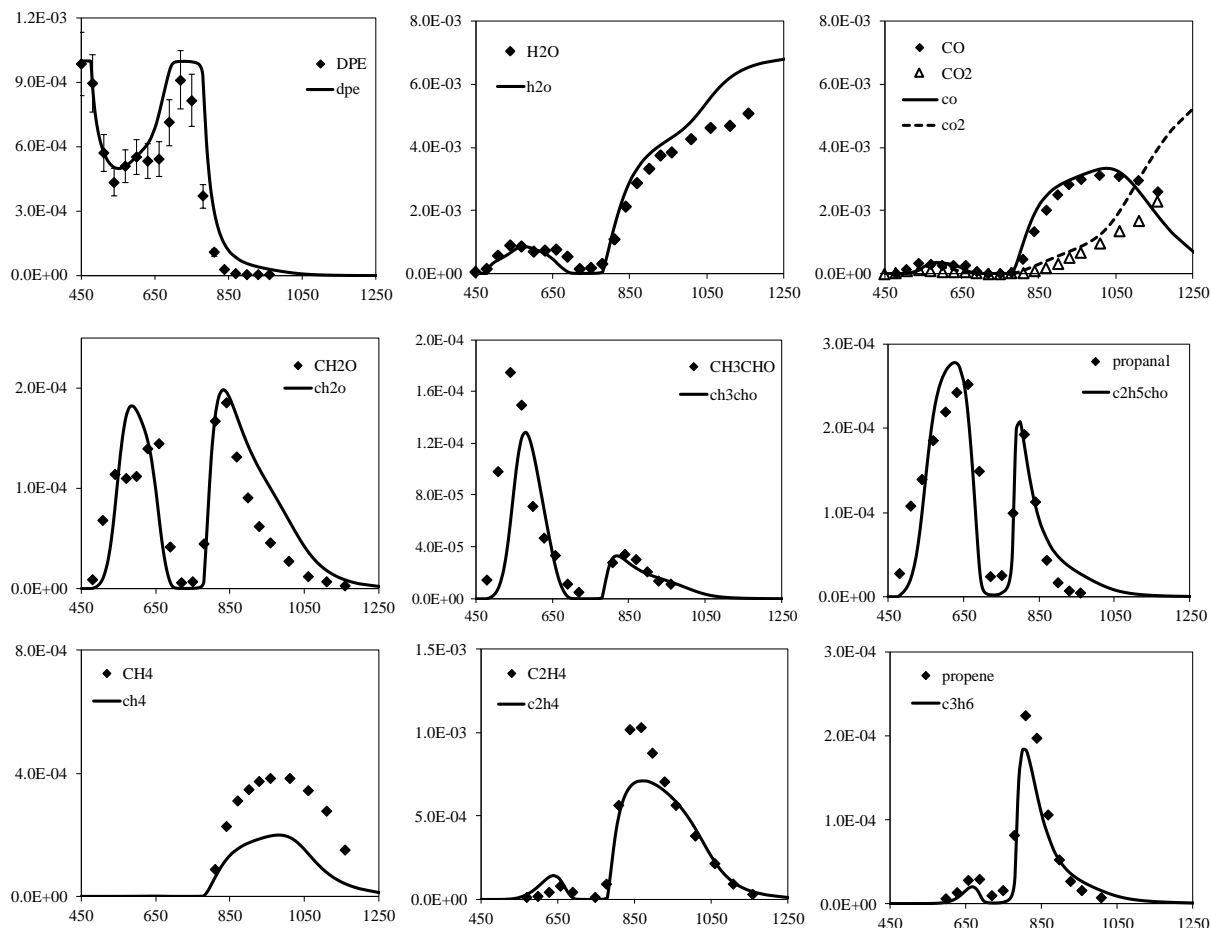
158

159 The most important low-temperature products observed were formaldehyde, propanal,
 160 acetaldehyde and propanoic acid. Formaldehyde is a typical marker of low-temperature
 161 reactivity of many fuels and is formed in large amounts in DPE oxidation as well. The typical
 162 oxygenated intermediate in the case of DPE is propanal. Similarly, butanal and acetaldehyde
 163 were observed in large quantities in DBE and DEE oxidation, respectively.

164 An interesting feature of ether oxidation turns out to be the formation of carboxylic
 165 acids. As an example, formic acid was identified and quantified in earlier studies by Curran et
 166 al. [26] in a flow reactor and by Dagaut et al. [27] in a jet-stirred reactor and more recently by
 167 Moshhammer et al. [28] in a jet-stirred reactor and by Wang et al. [29] in a flow reactor study.

168 In contrast to these studies, in their jet-stirred reactor study on low-temperature DME
169 oxidation by Rodriguez et al. [30], no formation of formic acid was reported.

170



171

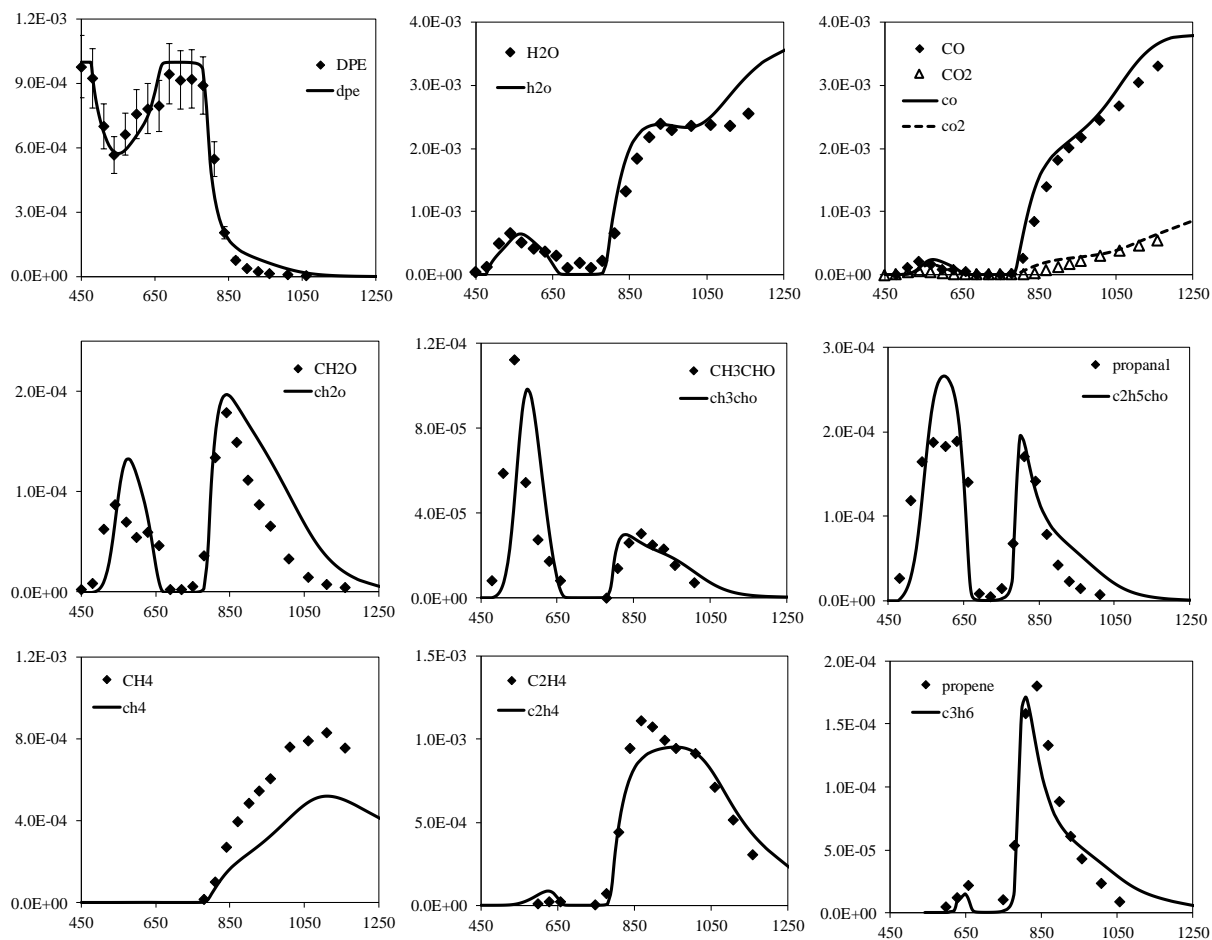
172 **Figure 3.** Mole fraction profiles as a function of reactor temperature ($\phi = 1$)

173

174 In our DEE study, acetic acid was quantified at low temperatures in considerable
175 quantities and in DBE oxidation butanoic acid was identified for some experiments but not
176 quantified. The formation routes of these acids are unclear and probably due to an
177 unconventional pathway followed by the radicals formed by ketohydroperoxide
178 decomposition. Formation of propanoic acid cannot be explained by analogy to the formic
179 acid formation pathway first proposed by Curran [26] and later calculated by Wang and co-

180 workers [29]. This formic acid pathway involves an internal hydrogen transfer from the acyl
 181 site of the $\cdot\text{OCH}_2\text{OCHO}$ radical (formed by C–O scission of the aldohydroperoxide) followed
 182 by its α -scission to formic acid and CO. However, in DPE oxidation the most abundant
 183 carbonylhydroperoxide is a ketohydroperoxide (shown in Fig 7 as c3oc31ohhket1) hence such
 184 a pathway is not possible. Therefore, although propanoic acid is quantified with a 125 ppm
 185 peak for $\phi = 0.5$ mixture and 16 ppm peak for $\phi = 4$ mixture, its profile is not simulated.

186

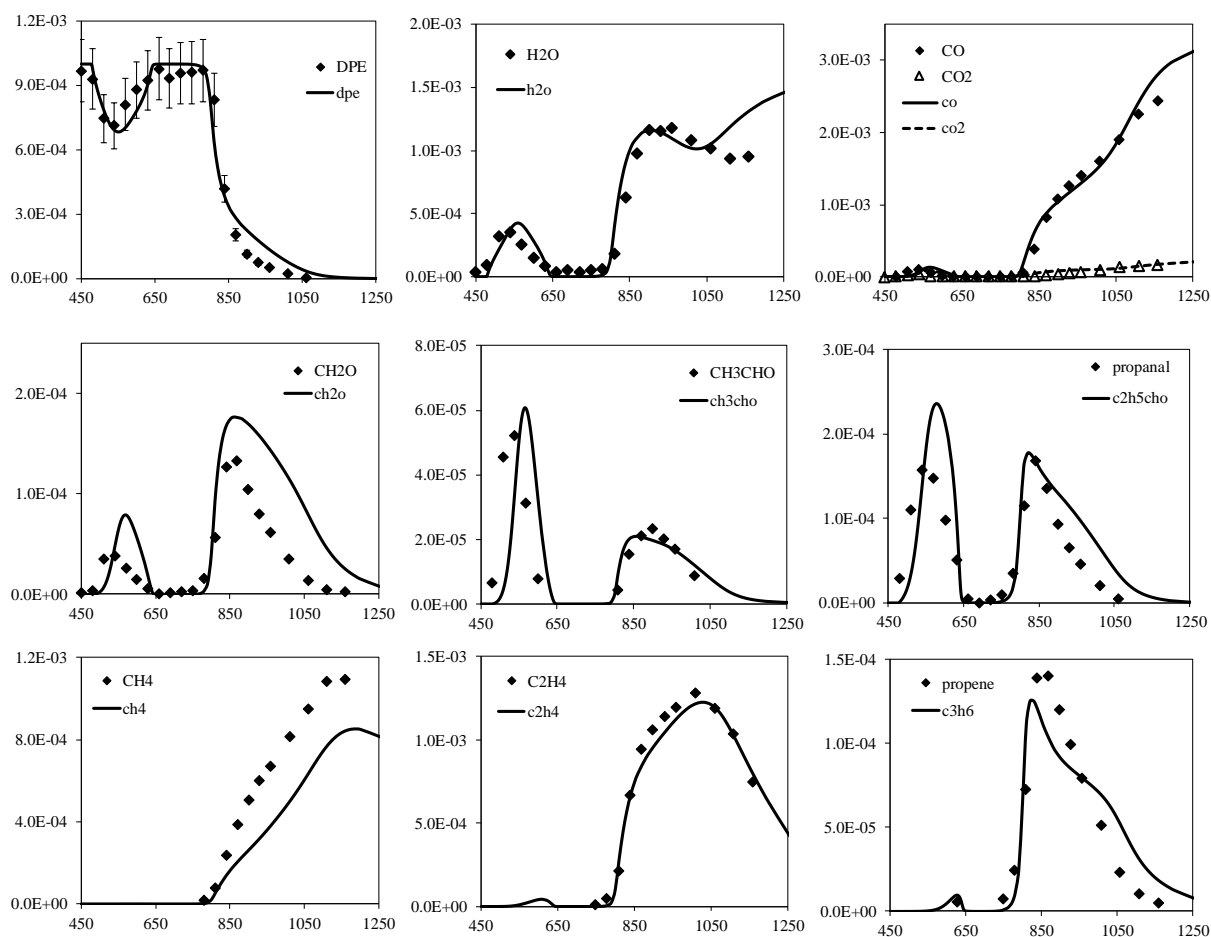


187

188 **Figure 4.** Mole fraction profiles as a function of reactor temperature ($\phi = 2$)

189

190 Generally speaking, for all conditions, kinetic model agrees reasonably well with the
 191 data. A factor of 1.5–2 discrepancy is observed with ethylene peak value and CO is slightly
 192 over-predicted in rich mixtures.



193

194

Figure 5. Mole fraction profiles as a function of reactor temperature ($\phi = 4$)

195

196 *Reaction pathways*

197 DPE can form three distinct fuel radicals, α -radical (dpe1), β - (dpe2) and γ - (dpe3) radicals.

198 C–H bond dissociation energies for DPE are calculated on G3B3 and CBS-QB3 levels using

199 Gaussian09 [31] and are presented below. According to this, the alpha C–H bond is the

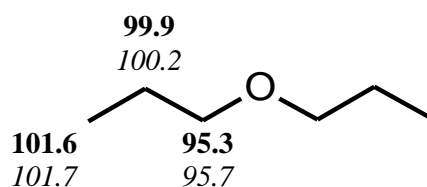
200 weakest and therefore the dpe1 radical is favored, which was naturally the case with DBE and

201 DEE. Also, note that the gamma C–H bond energy is similar to a primary C–H bond in

202 alkane, confirming the choice of analogy.

203

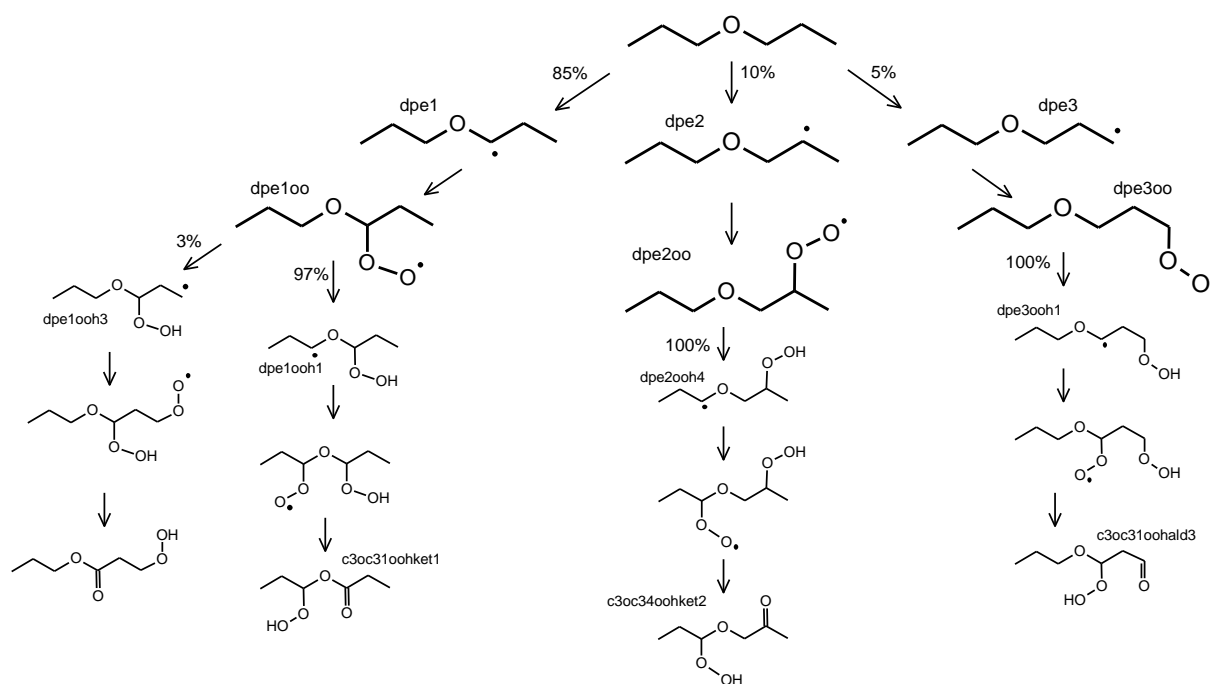
204



205

206 **Figure 6.** C–H bond dissociation energies of DPE calculated with G3B3 (bold) and
207 CBS-QB3 (italic)

208 Main reaction pathways are presented in Figure 7 for the low-temperature oxidation of
209 DPE, which is mainly consumed by H-abstraction reactions by OH radicals and this is the
210 case at any temperature. The percentages are evaluated at 500 K for the $\phi = 1$ mixture, as an
211 example.



212

213 **Figure 7.** Main reaction pathways at low temperatures (% are given at 500 K, $\phi = 1$)

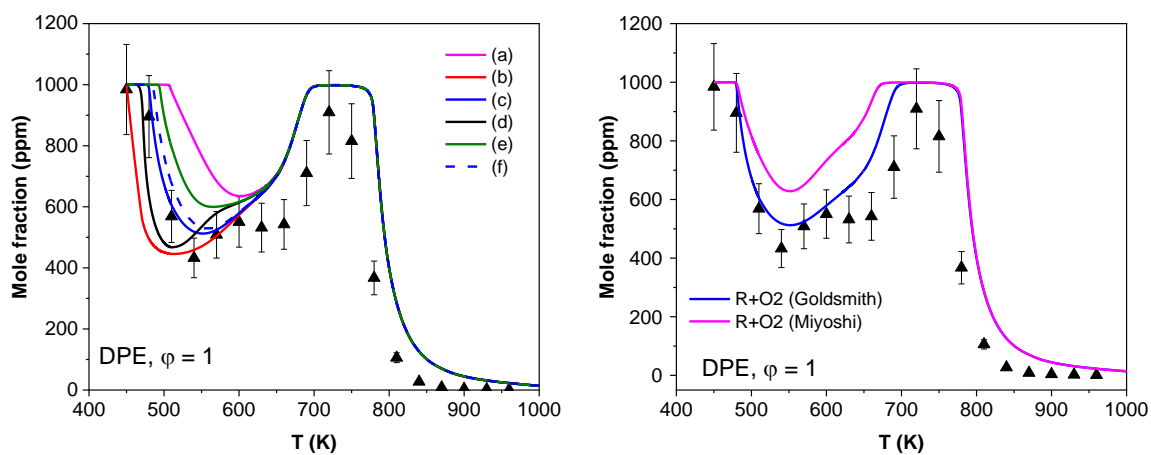
214

215 At low temperatures, addition of fuel radicals to molecular oxygen is dominant forming
216 the RO₂ radicals. The RO₂ radicals can go through isomerization (internal hydrogen transfer)
217 to form QOOH radicals. At these conditions the QOOH produced via 6-membered transition
218 states are favored and lead to the species and pathways as presented below. Propanal
219 formation at low temperature is via ketohydroperoxide decomposition, which is probably the

220 most important in low-temperature chemistry. In fact, this reaction is often written in one step
221 with chain branching fragments and an OH radical as products. The rate constant used for this
222 reaction in various mechanisms comes from an experimental study by Sahetchian et al. [32]
223 focusing on the decomposition of organic hydroperoxides, and it can be approximately
224 written as $k = 1 \times 10^{16} \exp(-43 \text{ kcal}/RT)$. A slightly different pre-exponential factor or
225 activation energy can be found in various literature mechanisms.

226 The Figure 8 shows the effect of this rate constant on the predictions of fuel mole
227 fraction. Activation energy of the KHP decomposition was modified by up to 6 kcal/mol. This
228 very low activation energy was proposed in the kinetic model of Cai et al. [33] on DBE
229 oxidation for all KHPs possible. The considerable effect of this rate constant on mole fraction
230 profiles can be clearly observed. We have also included the theoretical study of Goldsmith et
231 al. [34] on the decomposition of $\text{HOOCH}_2\text{CH}_2\text{CHO}$, via various channels. This rate constant
232 appears to be very close to the one obtained by reducing the original activation energy by 3
233 kcal, i.e. when using $1 \times 10^{16} \exp(-40 \text{ kcal}/RT)$ as the rate constant, which is therefore adopted
234 here. Furthermore, in order to highlight the effect of $\text{R} + \text{O}_2 \rightleftharpoons \text{RO}_2$ rate constant, we have
235 compared predictions with two theoretically calculated rate constants by Goldsmith [19] and
236 Miyoshi [35], both are widely used in kinetic mechanisms. Actually, this reversible reaction is
237 very sensitive to thermochemistry and note that in this study, group additivity is used. Also, as
238 is the case with the rate constants adopted from Villano et al. [20, 21] for this reaction class,
239 very often these calculations are done for alkanes. The similarities assumed are therefore done
240 compared to alkanes although the fuel is an ether. This probably adds an additional
241 uncertainty to the predictions.

242



243

244 **Figure 8.** Effect of KHP decomposition (left) and $R + O_2 \rightleftharpoons RO_2$ (right) reactions on model
 245 predictions. For the figure on the left : (a) assuming $E_a = 43$ kcal/mol for all KHP, (b)
 246 assuming $E_a = 37$ kcal/mol for all KHP, (c) assuming $E_a = 40$ kcal/mol for all KHP, (d)
 247 assuming $E_a = 37$ kcal/mol except for c3oc31oohket1, (e) assuming $E_a = 40$ kcal/mol except
 248 for c3oc31oohket1, (f) using the rate constant calculated by Goldsmith et al. [34] for the
 249 reaction $HOOCH_2CH_2CHO \rightarrow \bullet OCH_2CH_2CHO + \bullet OH$.

250

251

252

253

254

255

256

257

258

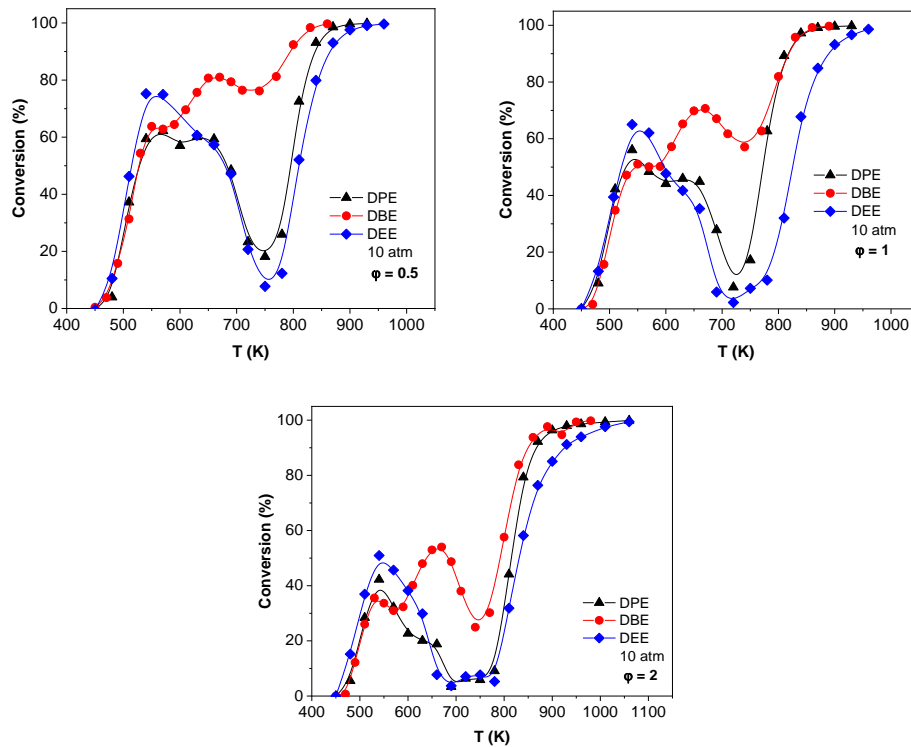
259

260

261

262

264



265

266

267

268 **Figure 9.** Comparison of the reactivity of DEE, DPE and DBE, all studied under same
 269 conditions (lines added to guide the eye)

270

271 Figure 9 illustrates the experimental fuel conversion of DEE, DPE and DBE, in order to
 272 compare their relative reactivity. On this plot one can clearly see the differences and
 273 similarities. All three ethers are very reactive, conversion begins right above 450 K, and they
 274 all exhibit a strong low-temperature reactivity and NTC behavior. On the other hand, DBE
 275 shows a clear double-NTC behavior, which is less pronounced in DPE oxidation and appears
 276 to be absent in the case of DEE. Among the three, DBE stands out with its very high
 277 conversion even in both NTC regions. For example, including the NTC region, DBE
 278 conversion is always higher than 60% for $\phi = 0.5$ mixture.

279 The particularity in DBE oxidation stems from the fact that even at these low temperatures,
280 owing to its long chain, formation of small radicals is possible. Its oxidation can produce
281 radicals such as n-propyl, mostly from the ketohydroperoxide $C_3H_7C(=O)OCH(OOH)C_3H_7$
282 decomposition. Decomposition of this ketohydroperoxide also produces butanal, which gives
283 n-propyl radicals by alpha-scission of its acyl radical at the low-intermediate temperature
284 range, and n-butyl radicals at intermediate temperatures. Therefore the low-intermediate
285 temperature regime in DBE oxidation is also controlled by the pathways followed by smaller
286 radicals that have their own low-temperature reactivity. On the other hand in DEE oxidation,
287 the chain is two carbon atoms smaller and these interactions do not take place. DPE, however,
288 is in midway between DEE and DBE and produces ethyl radicals in abundance during its
289 oxidation. Ethyl radicals add to molecular oxygen at lower temperatures and follow rather
290 dismutation pathways (producing ethanol, for example). They do not trigger an NTC type of
291 chemistry of their own like in DBE however they are more reactive than the methyl radicals
292 in DEE oxidation. Note that these observations hold for the investigated conditions of 1000
293 ppm initial fuel mole fraction, 10 atm and for a residence time of 700 ms and that at other
294 conditions reactivity profiles may be different. More details on DBE and DEE oxidation can
295 be found in the corresponding papers [6, 9].

296 At these temperatures thermochemistry is of crucial importance, hence the thermochemical
297 values (especially RO_2 , $QOOH$, $OOQOOH$) have to be as accurate as possible in addition to
298 the kinetics. Group additivity method may have its limits with such complex radicals. More
299 kinetic data is certainly useful for our understanding of the detailed chemistry, however we
300 should not neglect the effect of the uncertainties in thermochemistry, which are high with
301 such large and complex radicals.

302

303

304 **Summary**

305 In line with our previous studies on the oxidation of ethers, in the present work high-pressure
306 oxidation of di-n-propyl ether was studied in a jet-stirred reactor at various equivalence ratios
307 ($\varphi = 0.5\text{--}4$), for the first time. DPE exhibited an important low-temperature reactivity and a
308 double-NTC behavior, although to a lesser extent than that of DBE. A kinetic model was
309 developed in order to understand the oxidation patterns based on our previous efforts and
310 literature. This model shows a good agreement in general, however some discrepancies arise
311 from uncertainties in the rate parameters used. In order to extend this study to atmospheric
312 pressure, more experiments will be performed. Also, theoretical calculations could be useful
313 in interpreting the low-temperature oxidation behavior of the ether-related species.

314

315 **Acknowledgements**

316 Authors gratefully acknowledge funding received from Labex Caprysses (convention ANR-
317 11-LABX-0006-01).

318

319 **References**

320

- 321 [1] Yasunaga K, Gillespie F, Simmie JM, Curran HJ, Kuraguchi Y, Hoshikawa H, et al. A
322 Multiple Shock Tube and Chemical Kinetic Modeling Study of Diethyl Ether
323 Pyrolysis and Oxidation. *The Journal of Physical Chemistry A* 2010;114(34):9098-
324 109.
- 325 [2] Gillespie F, Metcalfe WK, Dirrenberger P, Herbinet O, Glaude P-A, Battin-Leclerc F,
326 et al. Measurements of flat-flame velocities of diethyl ether in air. *Energy*
327 2012;43(1):140-5.
- 328 [3] Werler M, Cancino LR, Schiessl R, Maas U, Schulz C, Fikri M. Ignition delay times
329 of diethyl ether measured in a high-pressure shock tube and a rapid compression
330 machine. *Proceedings of the Combustion Institute* 2015;35(1):259-66.
- 331 [4] Vin N, Herbinet O, Battin-Leclerc F. Diethyl ether pyrolysis study in a jet-stirred
332 reactor. *Journal of Analytical and Applied Pyrolysis* 2016;121:173-6.
- 333 [5] Tran L-S, Pieper J, Carstensen H-H, Zhao H, Graf I, Ju Y, et al. Experimental and
334 kinetic modeling study of diethyl ether flames. *Proceedings of the Combustion*
335 *Institute* 2017;36(1):1165-73.

- 336 [6] Serinyel Z, Lailliau M, Thion S, Dayma G, Dagaut P. An experimental chemical
337 kinetic study of the oxidation of diethyl ether in a jet-stirred reactor and
338 comprehensive modeling. *Combustion and Flame* 2018;193:453-62.
- 339 [7] Uygun Y. Ignition studies of undiluted diethyl ether in a high-pressure shock tube.
340 *Combustion and Flame* 2018;194:396-409.
- 341 [8] Tran L-S, Herbinet O, Li Y, Wullenkord J, Zeng M, Bräuer E, et al. Low-temperature
342 gas-phase oxidation of diethyl ether: Fuel reactivity and fuel-specific products.
343 *Proceedings of the Combustion Institute* 2019;37(1):511-9.
- 344 [9] Thion S, Togbé C, Serinyel Z, Dayma G, Dagaut P. A chemical kinetic study of the
345 oxidation of dibutyl-ether in a jet-stirred reactor. *Combustion and Flame* 2017;185:4-
346 15.
- 347 [10] Zhou C-W, Simmie JM, Curran HJ. An ab initio/Rice-Ramsperger-Kassel-Marcus
348 study of the hydrogen-abstraction reactions of methyl ethers, $\text{H}_3\text{COCH}_3\text{-x}(\text{CH}_3)_x$, $x =$
349 $0-2$, by [radical dot]OH; mechanism and kinetics. *Physical Chemistry Chemical*
350 *Physics* 2010;12(26):7221-33.
- 351 [11] Zhou C-W, Simmie JM, Curran HJ. Rate constants for hydrogen-abstraction by OH
352 from n-butanol. *Combustion and Flame* 2011;158(4):726-31.
- 353 [12] Zádor J, Miller JA. Hydrogen Abstraction From N-, I-Propanol And Nbutanol: A
354 Systematic Theoretical Approach. *7th US National Technical Meeting, Combust. Inst.*
355 *Atlanta, USA: Combust. Inst.; 2011:483-8*
- 356 [13] Seal P, Oyedepo G, Truhlar DG. Kinetics of the Hydrogen Atom Abstraction
357 Reactions from 1-Butanol by Hydroxyl Radical: Theory Matches Experiment and
358 More. *The Journal of Physical Chemistry A* 2013;117(2):275-82.
- 359 [14] Droege AT, Tully FP. Hydrogen atom abstraction from alkanes by hydroxyl. 5. n-
360 Butane. *The Journal of Physical Chemistry* 1986;90(22):5937-41.
- 361 [15] Ogura T, Miyoshi A, Koshi M. Rate coefficients of H-atom abstraction from ethers
362 and isomerization of alkoxyalkylperoxy radicals. *Physical Chemistry Chemical*
363 *Physics* 2007;9(37):5133-42.
- 364 [16] Tsang W. Chemical Kinetic Data Base for Combustion Chemistry. Part 3: Propane.
365 *Journal of Physical and Chemical Reference Data* 1988;17(2):887-951.
- 366 [17] Mendes J, Zhou C-W, Curran HJ. Rate Constant Calculations of H-Atom Abstraction
367 Reactions from Ethers by HO_2 Radicals. *The Journal of Physical Chemistry A*
368 2014;118(8):1300-8.
- 369 [18] Xu ZF, Park J, Lin MC. Thermal decomposition of ethanol. III. A computational study
370 of the kinetics and mechanism for the $\text{CH}_3+\text{C}_2\text{H}_5\text{OH}$ reaction. *The Journal of*
371 *Chemical Physics* 2004;120(14):6593-9.
- 372 [19] Goldsmith CF, Green WH, Klippenstein SJ. Role of $\text{O}_2 + \text{QOOH}$ in Low-
373 Temperature Ignition of Propane. 1. Temperature and Pressure Dependent Rate
374 Coefficients. *The Journal of Physical Chemistry A* 2012;116(13):3325-46.
- 375 [20] Villano SM, Huynh LK, Carstensen H-H, Dean AM. High-Pressure Rate Rules for
376 Alkyl + O_2 Reactions. 1. The Dissociation, Concerted Elimination, and Isomerization
377 Channels of the Alkyl Peroxy Radical. *The Journal of Physical Chemistry A*
378 2011;115(46):13425-42.
- 379 [21] Villano SM, Huynh LK, Carstensen H-H, Dean AM. High-Pressure Rate Rules for
380 Alkyl + O_2 Reactions. 2. The Isomerization, Cyclic Ether Formation, and β -Scission
381 Reactions of Hydroperoxy Alkyl Radicals. *The Journal of Physical Chemistry A*
382 2012;116(21):5068-89.
- 383 [22] Sakai Y, Ando H, Chakravarty HK, Pitsch H, Fernandes RX. A computational study
384 on the kinetics of unimolecular reactions of ethoxyethylperoxy radicals employing
385 CTST and VTST. *Proceedings of the Combustion Institute* 2015;35(1):161-9.

- 386 [23] Muller C, Michel V, Scacchi G, Côme GM. Thergas - A computer program for the
387 evaluation of thermochemical data of molecules and free radicals in the gas phase.
388 *Journal de chimie physique et de physico-chimie biologique* 1995;92(5):1154-78.
- 389 [24] Benson SW. *Thermochemical Kinetics*. New York: Wiley; 1976.
- 390 [25] Glarborg P, Kee RJ, Grcar JF, Miller JA. PSR: A Fortran Program for Modeling Well-
391 Stirred Reactors, Report No. SAND86-8209, Sandia National Laboratories,
392 Albuquerque, NM. 1986.
- 393 [26] Curran HJ, Fischer SL, Dryer FL. The reaction kinetics of dimethyl ether. II: Low-
394 temperature oxidation in flow reactors. *International Journal of Chemical Kinetics*
395 2000;32(12):741-59.
- 396 [27] Dagaut P, Luche J, Cathonnet M. The Low Temperature Oxidation of DME and
397 Mutual Sensitization of the Oxidation of DME and Nitric Oxide: Experimental and
398 Detailed Kinetic Modeling. *Combustion Science and Technology* 2001;165(1):61-84.
- 399 [28] Moshhammer K, Jasper AW, Popolan-Vaida DM, Lucassen A, Diévert P, Selim H, et
400 al. Detection and Identification of the Keto-Hydroperoxide (HOOCH₂OCHO) and
401 Other Intermediates during Low-Temperature Oxidation of Dimethyl Ether. *The*
402 *Journal of Physical Chemistry A* 2015.
- 403 [29] Wang Z, Zhang X, Xing L, Zhang L, Herrmann F, Moshhammer K, et al. Experimental
404 and kinetic modeling study of the low- and intermediate-temperature oxidation of
405 dimethyl ether. *Combustion and Flame* 2015;162(4):1113-25.
- 406 [30] Rodriguez A, Frottier O, Herbinet O, Fournet R, Bounaceur R, Fittschen C, et al.
407 Experimental and Modeling Investigation of the Low-Temperature Oxidation of
408 Dimethyl Ether. *The Journal of Physical Chemistry A* 2015;119(28):7905-23.
- 409 [31] Frisch MJT, G. W.; Schlegel, H. B.; Scuseria, G. E.; Robb, M. A.; Cheeseman, J. R.;
410 Scalmani, G.; Barone, V.; Mennucci, B.; Petersson, G. A.; Nakatsuji, H.; Caricato, M.;
411 Li, X.; Hratchian, H. P.; Izmaylov, A. F.; Bloino, J.; Zheng, G.; Sonnenberg, J. L.;
412 Hada, M.; Ehara, M.; Toyota, K.; Fukuda, R.; Hasegawa, J.; Ishida, M.; Nakajima, T.;
413 Honda, Y.; Kitao, O.; Nakai, H.; Vreven, T.; Montgomery, J. A., Jr. ; Peralta, J. E.;
414 Ogliaro, F.; Bearpark, M.; Heyd, J. J.; Brothers, E.; Kudin, K. N.; Staroverov, V. N.;
415 Kobayashi, R.; Normand, J.; Raghavachari, K.; Rendell, A.; Burant, J. C.; Iyengar, S.
416 S.; Tomasi, J.; Cossi, M.; Rega, N.; Millam, N. J.; Klene, M.; Knox, J. E.; Cross, J. B.;
417 Bakken, V.; Adamo, C.; Jaramillo, J.; Gomperts, R.; Stratmann, R. E.; Yazyev, O.;
418 Austin, A. J.; Cammi, R.; Pomelli, C.; Ochterski, J. W.; Martin, R. L.; Morokuma, K.;
419 Zakrzewski, V. G.; Voth, G. A.; Salvador, P.; Dannenberg, J. J.; Dapprich, S.;
420 Daniels, A. D.; Farkas, Ö.; Foresman, J. B.; Ortiz, J. V.; Cioslowski, J.; Fox, D. J.
421 *Gaussian 09, Revision D.01*. Wallingford CT: Gaussian, Inc.; 2009.
- 422 [32] Sahetchian KA, Rigny R, Tardieu de Maleissye J, Batt L, Anwar Khan M, Mathews S.
423 The pyrolysis of organic hydroperoxides (ROOH). *Symposium (International) on*
424 *Combustion* 1992;24(1):637-43.
- 425 [33] Cai L, Sudholt A, Lee DJ, Egolfopoulos FN, Pitsch H, Westbrook CK, et al. Chemical
426 kinetic study of a novel lignocellulosic biofuel: Di-n-butyl ether oxidation in a laminar
427 flow reactor and flames. *Combustion and Flame* 2014;161(3):798-809.
- 428 [34] Goldsmith CF, Burke MP, Georgievskii Y, Klippenstein SJ. Effect of non-thermal
429 product energy distributions on ketohydroperoxide decomposition kinetics.
430 *Proceedings of the Combustion Institute* 2015;35(1):283-90.
- 431 [35] Miyoshi A. Systematic Computational Study on the Unimolecular Reactions of
432 Alkylperoxy (RO₂), Hydroperoxyalkyl (QOOH), and Hydroperoxyalkylperoxy
433 (O₂QOOH) Radicals. *The Journal of Physical Chemistry A* 2011;115(15):3301-25.
- 434
435